Journal of Scientific Computing, Vol. 1, No. 1, 1986

Boundary Conditions for Incompressible Flows

Steven A. Orszag,[1] Moshe Israeli,[1] and Michel O. Deville[2]

Received June 23, 1986

A general framework is presented for the formulation and analysis of rigid no-slip boundary conditions for numerical schemes for the solution of the incompressible Navier–Stokes equations. It is shown that fractional-step (splitting) methods are prone to introduce a spurious numerical boundary layer that induces substantial time differencing errors. High-order extrapolation methods are analyzed to reduce these errors. Both improved pressure boundary condition and velocity boundary condition methods are developed that allow accurate implementation of rigid no-slip boundary conditions.

KEY WORDS: Computational fluid dynamics; splitting methods; Poisson equation; fractional step methods; extrapolation methods; time-stepping methods; incompressible flows; boundary conditions.

1. INTRODUCTION

In this paper, we address the numerical implementation of no-slip boundary conditions for incompressible flows. In particular, simple techniques to achieve high-order accurate time integrations of the incompressible flow equations are developed.

The Navier–Stokes equations for incompressible flow are

$$\frac{\partial \mathbf{v}}{\partial t} + \nabla p = -\mathbf{v} \cdot \nabla \mathbf{v} + \nu \nabla^2 \mathbf{v} + \mathbf{f} \qquad (\mathbf{x} \in D) \tag{1.1}$$

$$\nabla \cdot \mathbf{v} = 0 \qquad (\mathbf{x} \in D) \tag{1.2}$$

where $\mathbf{v}(\mathbf{x}, t)$ is the velocity field at $\mathbf{x}, t$; $p(\mathbf{x}, t)$ is the pressure; ν is the kinematic viscosity; and $\mathbf{f}(\mathbf{x}, t)$ is an external force. The (constant) density is assumed to be unity. If the boundaries of the region D in which the flow

[1] Applied and Computational Mathematics, Princeton University, Princeton, New Jersey 08544.

[2] Université de Louvain, Louvain, Belgium.

0885-7474/86/0600-0075$05.00/0

satisfying (1.1)–(1.2) occurs are stationary and if $\nu > 0$, then the appropriate boundary conditions are the no-slip conditions

$$\mathbf{v}(\mathbf{x}, t) = 0 \qquad (\mathbf{x} \in \partial D) \tag{1.3}$$

One of the central questions to be addressed here is the calculation of the pressure p in numerical solutions of (1.1)–(1.3). The pressure in (1.1) may be considered a Lagrange multiplier that ensures satisfaction of the (kinematical) incompressibility constraint (1.2) everywhere in D. The most obvious way to obtain an equation for p is to take the divergence of (1.1) and apply (1.2), which gives the Poisson equation

$$\nabla^2 p = -\nabla \cdot (\mathbf{v} \cdot \nabla)\, \mathbf{v} + \nabla \cdot \mathbf{f} \qquad (\mathbf{x} \in D) \tag{1.4}$$

A warning of possible trouble in the numerical solution (1.1)–(1.3) is given when boundary conditions for (1.4) are sought (Orszag and Israeli, 1974). Applying the boundary conditions (1.3) to (1.1) gives

$$\nabla p = \nu \nabla^2 \mathbf{v} + \mathbf{f} \qquad (\mathbf{x} \in \partial D) \tag{1.5}$$

so both Dirichlet and Neumann conditions for p are available if $\mathbf{v}$ is known. In numerical integrations of (1.1)–(1.3), it is not obvious which of these boundary conditions to use, and the equations for p may appear to be overdetermined.

For inviscid flow, the problem discussed in the last paragraph does not occur, since inviscid flow permits slip at the boundary; the no-slip conditions (1.3) are replaced by

$$\mathbf{v} \cdot \mathbf{n} = 0 \qquad (\mathbf{x} \in \partial D) \tag{1.6}$$

where $\mathbf{n}$ is normal to ∂D at $\mathbf{x}$. Thus, only the normal component of (1.5) holds and Neumann boundary conditions are appropriate for (1.4). In numerical practice, it is often argued that Neumann conditions on p are also most appropriate for high-Reynolds-number flows, presumably because of the inviscid analogy. We shall see below that there are both theoretical and practical considerations that favor this choice of boundary condition.

The ambiguity regarding boundary conditions on p can be avoided if the pressure is eliminated from (1.1)–(1.3). Applying the operator $\nabla \times \nabla \times$ to (1.1) gives, using (1.2),

$$\frac{\partial}{\partial t} \nabla^2 \mathbf{v} = \nabla \times [\nabla \times (\mathbf{v} \cdot \nabla)\, \mathbf{v}] + \nu \nabla^4 \mathbf{v} - \nabla \times (\nabla \times \mathbf{f}) \qquad (\mathbf{x} \in D) \tag{1.7}$$

For flow in a plane channel, implicit time stepping of the linear terms in (1.7) gives a fourth-order equation for the component v_n of $\mathbf{v}$ in the direction $\mathbf{n}$ of the normal to the channel walls. Solving this fourth-order equation requires imposition of four boundary conditions on v_n. Two of these conditions are immediately available, namely $v_n = 0$ at the two boundaries of the channel. The other two conditions follow from the incompressibility constraint (1.2); since $\mathbf{v} = 0$ at the walls, $(\mathbf{n} \times \nabla)\,\mathbf{v} = 0$ so $\nabla \cdot \mathbf{v} = 0$ implies that $\partial v_n / \partial n = 0$ there. Once v_n is known, the other components of $\mathbf{v}$ are obtained using incompressibility and the equation for the component of vorticity in direction $\mathbf{n}$. Indeed, if $\nabla_H = \nabla - \mathbf{n}(\partial/\partial n)$ is the two-dimensional gradient operator parallel to the channel walls, then $\nabla_H \cdot \mathbf{v} = -\partial v_n / \partial n$, while $\mathbf{n} \cdot \nabla_H \times \mathbf{v} = \omega_n$ is the normal vorticity. Then Weyl's lemma implies that $\mathbf{n} \times \mathbf{v}$ is determined fully.

In general three-dimensional geometries, the equations (1.7) are coupled and are not so easily solved. Then, implicit time stepping of the linear terms in (1.1)–(1.3) leads to a coupled sixth-order system for $\mathbf{v}, p$.

We shall see that time, rather than space, discretization is the key step in the numerical treatment of the pressure term in the Navier–Stokes equations. This is due to the incomplete parabolic nature of the system [in the sense that the Poisson equation (1.4) for the pressure is a diagnostic, rather than a prognostic, equation]. A general high-order formulation is a good framework for all the time stepping schemes under consideration. Let us write the Navier–Stokes equations as

$$\partial \mathbf{v} / \partial t = -\nabla p + \mathbf{L}(\mathbf{v}) + \mathbf{N}(\mathbf{v}) \tag{1.8}$$

$$Q = \nabla \cdot \mathbf{v} = 0 \tag{1.9}$$

where the linear term $\mathbf{L}(\mathbf{v})$ is given by

$$\mathbf{L}(\mathbf{v}) = \nu[\nabla(\nabla \cdot \mathbf{v}) - \nabla \times (\nabla \times \mathbf{v})]$$

and the nonlinear term $\mathbf{N}(\mathbf{v})$ is given by

$$\mathbf{N}(\mathbf{v}) = -\mathbf{v} \cdot \nabla \mathbf{v}$$

Integrating (1.8) over a time step gives

$$\mathbf{v}^{n+1} - \mathbf{v}^n = -\int_{t_n}^{t_{n+1}} \nabla p \, dt + \int_{t_n}^{t_{n+1}} \mathbf{L}(\mathbf{v}) \, dt + \int_{t_n}^{t_{n+1}} \mathbf{N}(\mathbf{v}) \, dt \tag{1.10}$$

where the superscript index n indicates time level $n \, \Delta t$. We can write

$$\int_{t_n}^{t_{n+1}} \nabla p \, dt = \nabla \int_{t_n}^{t_{n+1}} p \, dt = \Delta t \, \nabla \bar{p}^{n+1}$$

so that $\bar{p}^{n+1}$ is the scalar field that maintains incompressibility at time $(n+1)\,\Delta t$. The remaining two integrals on the right side of (1.10) may be approximated using Adams–Bashforth time differencing schemes of appropriate order. For example, at jth order, the nonlinear term is computed explicitly as

$$\int_{t_n}^{t_{n+1}} \mathbf{N}(\mathbf{v})\,dt = \sum_{k=0}^{j-1} \mathbf{N}(\mathbf{v}^{n-k})\,\gamma_k\,\Delta t \equiv \bar{\mathbf{N}}^n\,\Delta t$$

for suitable weights γ_k. The linear term may be evaluated by an implicit scheme for improved stability:

$$\begin{aligned}\int_{t_n}^{t_{n+1}} \mathbf{L}(\mathbf{v})\,dt &= \beta\mathbf{L}(\mathbf{v}^{n+1})\,\Delta t + \sum_{k=0}^{j-2} \mathbf{L}(v^{n-k})\,\beta_k\,\Delta t \\ &= \beta\mathbf{L}(\mathbf{v}^{n+1})\,\Delta t + \bar{\mathbf{L}}^n\,\Delta t\end{aligned}$$

for suitable weights β, β_k. It follows that

$$\mathbf{v}^{n+1} - \beta\,\Delta t\,\mathbf{L}(\mathbf{v}^{n+1}) = \mathbf{v}^n - \Delta t\,\nabla\bar{p}^{n+1} + \Delta t\,\mathbf{F}^n; \qquad \mathbf{F}^n = \bar{\mathbf{N}}^n + \bar{\mathbf{L}}^n \tag{1.11}$$

Equations (1.11) together with $\nabla\cdot\mathbf{v}^{n+1} = 0$ are a coupled system. This system leads to difficult computational problems, equivalent to that of solving for steady Stokes flow at each time step. Therefore, it is important to develop simplified and efficiently solvable numerical approximations. This can be done by attempting to decouple the pressure computation from that of the velocity, thereby reducing the problem to a system of separately solvable second-order equations. Three steps are required in order to complete the decoupling.

The first step was already taken by explicit evaluation of the nonlinear terms $\bar{\mathbf{N}}_n$, which involves only previously known time levels. The second step is the derivation of the appropriate equations for the pressure. It involves the well-known step of taking the divergence of (1.1) to get (1.4). The third step involves the implicit computation of viscous effects. While these steps have been well known to practitioners of computational fluid dynamics, it is still mysterious how and why they work. We will reinterpret this approach and shed new light on its consequences.

Taking the divergence of (1.11) gives

$$\frac{Q^{n+1}}{\Delta t} - \beta\nu\,\nabla^2 Q^{n+1} = \frac{Q^n}{\Delta t} + \nabla\cdot\mathbf{F}^n - \nabla^2\bar{p}^{n+1} \tag{1.12}$$

If the goal is to obtain $Q^{n+1} = 0$ and we assume that all velocities are known at level n, then (1.12) shows that $\bar{p}^{n+1}$ must satisfy

$$\nabla^2\bar{p}^{n+1} = \nabla\cdot\mathbf{F}^n + \frac{1}{\Delta t}\,Q^n \tag{1.13}$$

In turn, (1.12) and (1.13) show that Q^{n+1} satisfies

$$Q^{n+1} - \beta\nu\,\Delta t\,\nabla^2 Q^{n+1} = 0 \tag{1.14}$$

However, (1.14) implies that $Q^{n+1} \equiv 0$ throughout D only if the boundary conditions are such that Q^{n+1} or $\partial Q^{n+1}/\partial n$ vanishes on the boundary.

Even if $Q^{n+1} \neq 0$ on the boundary, (1.14) shows that, as $\nu\,\Delta t \to 0$, Q^{n+1} decays exponentially to zero in the interior of the domain D beyond a (numerical) boundary layer of thickness $(\nu\,\Delta t)^{1/2}$. Furthermore, since (1.14) is elliptic, standard maximum theorems ensure that the boundary values of Q^{n+1} dominate all interior values. Thus, the crux of the problem of controlling Q^{n+1} lies with control of its boundary values.

An alternative approach to obtain equations for $\bar{p}^{n+1}$ is to assume that $Q^n = Q^{n+1} = 0$ in (1.12). Then (1.13) is replaced by

$$\nabla^2 \bar{p}^{n+1} = \nabla \cdot \mathbf{F}^n \tag{1.15}$$

However, if $\bar{p}^{n+1}$ is determined by (1.15), then (1.12) shows that Q actually satisfies

$$\frac{Q^{n+1} - Q^n}{\Delta t} = \beta\nu\,\nabla^2 Q^{n+1} \tag{1.16}$$

This time-discretized parabolic equation is a prognostic equation for the divergence. The behavior of its solutions controls the evolution of the divergence field in the numerical computation. Clearly there is the solution $Q^n = Q^{n+1} \equiv 0$ in D, but this solution is only achieved if suitable initial *and* boundary conditions hold. With the parabolic equation (1.16), the numerical boundary layer of thickness $(\nu\,\Delta t)^{1/2}$ around ∂D typically disappears and is replaced by smooth diffusion of the divergence from the boundary into the interior of the domain. There is a maximum theorem for (1.16) which shows that the divergence at step $n+1$ is dominated by the boundary divergence or by the divergence at step n. If the diameter of the domain D is L, then it requires a time of order L^2/ν for the effect of initially nonzero Q^0 to diffuse out and for the magnitude of Q^n in D to reflect the boundary conditions on ∂D alone.

It is now clear that a crucial step in the determination of the pressure involves the imposition of the boundary conditions. This is the main subject of this paper. It is also clear now why "elliptic" schemes of the form (1.13)–(1.14) are superior to "parabolic" schemes of the form (1.15)–(1.16). The former schemes forget the effect of initial conditions immediately and Q in D reflects only the effect of boundary conditions on ∂D. However, the absence of the numerical boundary layer of width $(\nu\,\Delta t)^{1/2}$ in the parabolic

schemes means that extrapolation methods (see Section 6) can be easily used to increase the order of accuracy of the methods.

In Section 2, we present a one-dimensional problem that models multidimensional fluid dynamics. It gives a convenient framework for the analysis of methods to solve incompressible flow problems. In Sections 3 and 4, we survey the properties of several *semidiscrete* numerical approximations to incompressible flows. Here semidiscrete means that the time coordinate is discretized but the spatial coordinates remain continuous. In Section 5, we illustrate the analysis of the schemes outlined in Sections 3 and 4 using the model problem of Section 2. In Section 6, we introduce extrapolation methods that can yield higher order results with the splitting methods of Section 4. Then, in Section 7, we present the main results of this paper, namely, new methods with improved boundary conditions that are both accurate and efficient. In Section 8, we conclude with some recommendations for efficient and accurate solution of incompressible flow problems. In the Appendices, some additional schemes are analyzed. The reader who is mainly interested in computational efficiency may wish to refer directly to Section 7.

2. A ONE-DIMENSIONAL MODEL OF INCOMPRESSIBLE FLOW

A one-dimensional linear model that embodies the essential features of the incompressibility and viscous terms of the Navier–Stokes equations is obtained by considering a solution to the two-dimensional Stokes equations of the form

$$\mathbf{v} = \left(u(x, t)\, e^{iky}, v(x, t)\, e^{iky}\right), \qquad p = p(x, t)\, e^{iky}$$

for some real wavenumber k. The equations satisfied by (u, v, p) are

$$\frac{\partial u}{\partial t} = -\frac{\partial p}{\partial x} + \nu(u_{xx} - k^2 u) \tag{2.1}$$

$$\frac{\partial v}{\partial t} = -ikp + \nu(v_{xx} - k^2 v) \tag{2.2}$$

$$\frac{\partial u}{\partial x} + ikv = 0 \tag{2.3}$$

for $-1 \leqslant x \leqslant 1$. The boundary conditions are

$$u(\pm 1, t) = v(\pm 1, t) = 0 \tag{2.4}$$

which simulate rigid no-slip boundary conditions.

The solution to an initial-value problem for (2.1)–(2.4) can be expressed in terms of normal modes of the form

$$(u, v, p)(x, t) = e^{\sigma t}(\hat{u}, \hat{v}, \hat{p})(x) \tag{2.5}$$

Substitution of (2.5) into (2.1)–(2.3) and elimination of $\hat{v}$ and $\hat{p}$ gives

$$\sigma(D^2 - k^2)\,\hat{u} = \nu(D^2 - k^2)^2\,\hat{u} \qquad (-1 < x < 1) \tag{2.6}$$

with $\hat{u}(\pm 1) = D\hat{u}(\pm 1) = 0$, where $D = d/dx$.

The exact solutions to (2.6) are either symmetric in x:

$$\hat{u}(x) = \cos\mu\,\cosh kx - \cosh k\,\cos\mu x \tag{2.7}$$

or antisymmetric:

$$\hat{u}(x) = \sin\mu\,\sinh kx - \sinh k\,\sin\mu x \tag{2.8}$$

Here

$$\mu = (-\sigma/\nu - k^2)^{1/2} \tag{2.9}$$

satisfies the eigenvalue relations

$$k\tanh k = -\mu\tan\mu \tag{2.10}$$

for (2.7) and

$$k\coth k = \mu\cot\mu \tag{2.11}$$

for (2.8). These eigenmodes are complete on the interval $|x| \leqslant 1$. Some values of μ and σ for low-lying modes with $k = 1$ and 10 are listed in Table I. All the eigenvalues σ are real and negative, indicating stability for $\nu > 0$. In Fig. 1, we plot $\hat{u}(x)$, $i\hat{v}(x)$, $\hat{p}(x)$, and $D\hat{p}(x)$ as functions of x for the lowest symmetric mode with $\nu = k = 1$.

Table I. Decay Rates of Slowest Decaying Normal Modes of (2.1)–(2.4) with $k = 1$ and $k = 10$

	$k = 1$		$k = 10$	
Symmetry[a]	μ	σ/ν	μ	σ/ν
S	2.883356	−9.3137	1.743402	−103.0394
A	4.423864	−20.5706	3.476140	−112.0836
S	6.160178	−38.9478	5.191217	−126.9487
A	7.684753	−60.0554	6.886235	−147.4202
S	9.343447	−88.3000	8.562068	−173.3090

[a] S indicates a symmetric (in x) mode; A indicates an antisymmetric mode.

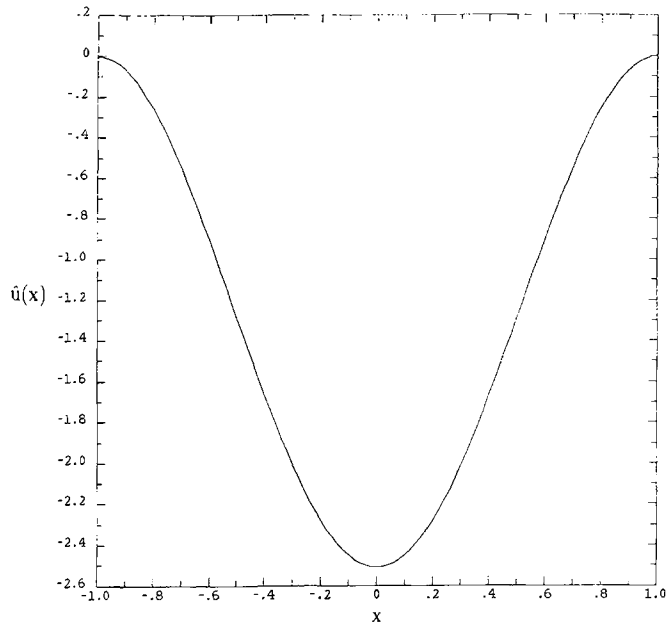

(a)

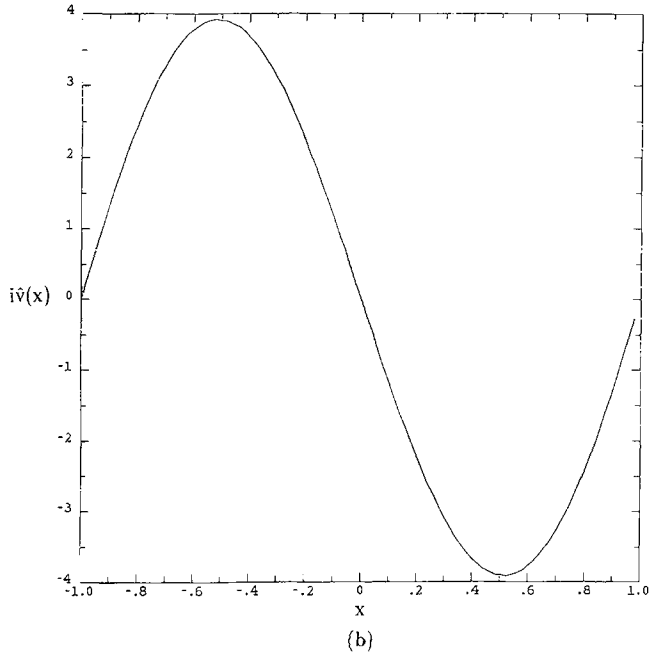

(b)

Fig. 1. Plots of the normal mode of the system (2.1)–(2.4) with $\nu = k = 1$. (a) $\hat{u}(x)$; (b) $i\hat{v}(x)$; (c) $\hat{p}(x)$; (d) $D\hat{p}(x)$.

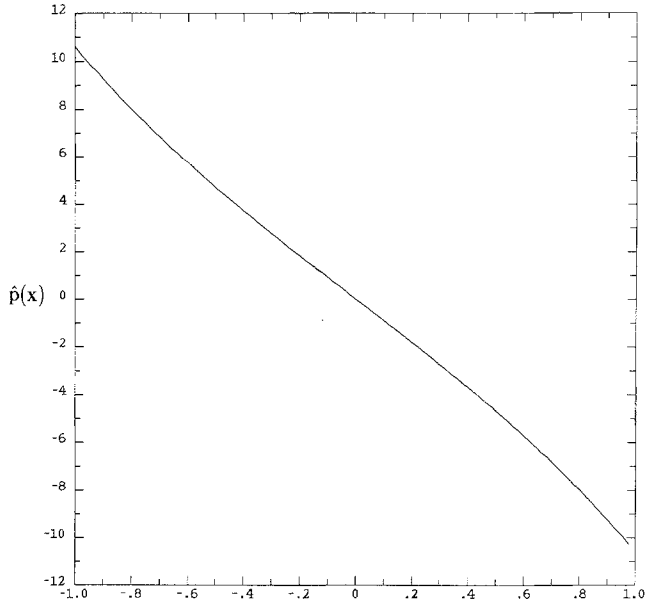

(c)

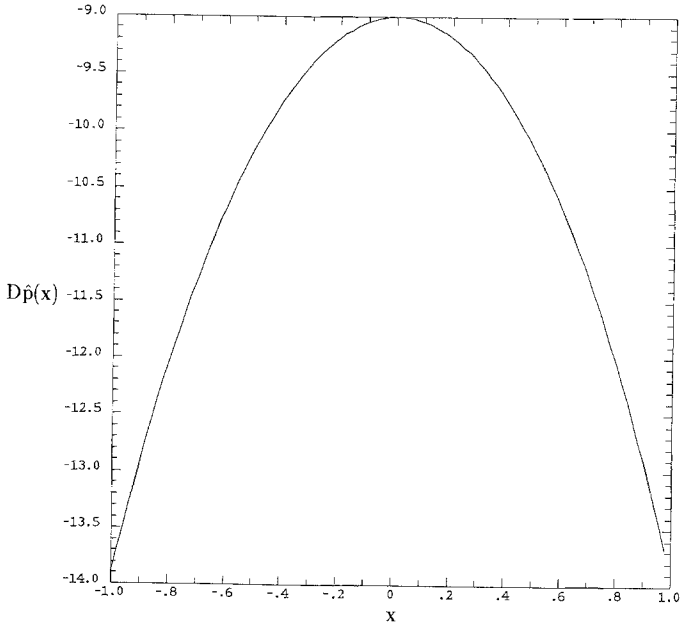

(d)

Fig. 1. Continued.

3. SEMIDISCRETE IMPLICIT COUPLED METHODS

In this section we give two semidiscrete schemes for the solution of incompressible fluid dynamics. The schemes are discrete in time but continuous in space.

3.1. Full Implicit Time Differencing

Here the system (2.1)–(2.4) is approximated by backward Euler time differencing:

$$\frac{u^{n+1}-u^n}{\Delta t} = -Dp^{n+1} + \nu(D^2-k^2)\,u^{n+1} \tag{3.1}$$

$$\frac{v^{n+1}-v^n}{\Delta t} = -ikp^{n+1} + \nu(D^2-k^2)\,v^{n+1} \tag{3.2}$$

$$Du^{n+1} + ikv^{n+1} = 0 \tag{3.3}$$

It follows that

$$\frac{1}{\Delta t}(D^2-k^2)\,u^{n+1} - \nu(D^2-k^2)^2\,u^{n+1} = -\frac{ik}{\Delta t}Dv^n - \frac{k^2}{\Delta t}u^n \tag{3.4}$$

with $u^{n+1} = Du^{n+1} = 0$ at $x = \pm 1$. Comparison of (3.4) with (2.6) shows that there are eigenmode solutions to (3.1)–(3.3) of the form

$$(u^n, v^n, p^n) = \kappa^n(\tilde{u}, \tilde{v}, \tilde{p}) \tag{3.5}$$

with

$$\kappa = 1/(1-\sigma\,\Delta t) \tag{3.6}$$

where σ is the exact eigenvalue obtained from (2.9)–(2.11) and $(\tilde{u}, \tilde{v}, \tilde{p})$ are identical to $(\hat{u}, \hat{v}, \hat{p})$ obtained in Section 2. The time dependence of (u^n, v^n, p^n) is proportional to

$$\kappa^n = \exp(\tilde{\sigma} n\,\Delta t), \qquad \tilde{\sigma} = \frac{1}{\Delta t}\ln\kappa \approx \sigma + \frac{1}{2}\sigma^2\,\Delta t + O(\Delta t^2) \tag{3.7}$$

so the growth rate $\tilde{\sigma}$ for this scheme is in error by $O(\Delta t)$. Also, since $\sigma < 0$, $\kappa < 1$, the scheme is unconditionally stable. Thus, the normal mode analysis demonstrates the stability and convergence of this implicit semidiscrete scheme as $\Delta t \to 0$.

Higher order implicit time differencing leads to similar results with higher order approximations κ to $\exp(\sigma \Delta t)$. For example, the Crank–Nicolson scheme is considered next.

3.2. Crank–Nicolson Time Differencing

$$\frac{u^{n+1}-u^n}{\Delta t} = -Dp^{n+1/2} + \frac{1}{2}\nu(D^2-k^2)(u^{n+1}+u^n) \tag{3.8}$$

$$\frac{v^{n+1}-v^n}{\Delta t} = -ikp^{n+1/2} + \frac{1}{2}\nu(D^2-k^2)(v^{n+1}+v^n) \tag{3.9}$$

$$Du^{n+1} + ikv^{n+1} = 0 \tag{3.10}$$

with $u^{n+1} = v^{n+1} = 0$ at $x = \pm 1$ is both unconditionally stable and accurate to $O(\Delta t^2)$. Indeed, normal mode solutions exist in the form (3.5) with $\kappa = (1 + \frac{1}{2}\sigma \Delta t)/(1 - \frac{1}{2}\sigma \Delta t)$, so $|\kappa| < 1$ since $\sigma < 0$.

Algorithms to implement these two schemes efficiently for finite-difference and spectral methods have been discussed by Gottlieb and Orszag (1977), Moin and Kim (1980), Kleiser and Schumann (1980), and Gottlieb *et al.* (1984). One way is to use a Green's function (influence matrix) method. This method is particularly easy to understand for the present one-dimensional model. The generalization of this Green's function method to nonseparable multidimensional problems is straightforward, but computationally expensive, especially in three space dimensions. Therefore, we shall seek more effective computational schemes for such problems in Sections 4 and 6.

Equation (3.4) is solved using Green's functions by first introducing the auxiliary variable ζ by

$$\zeta^{n+1} = (D^2 - k^2)\, u^{n+1}$$

Then

$$u^{n+1} = u_p^{n+1} + \alpha_+^{n+1} u_+ + \alpha_-^{n+1} u_- \tag{3.11}$$

where the particular solution u_p^{n+1} satisfies

$$\begin{aligned} \frac{1}{\Delta t}\zeta_p^{n+1} - \nu(D^2-k^2)\,\zeta_p^{n+1} &= \frac{ik}{\Delta t} Dv^n - \frac{k^2}{\Delta t} u^n \qquad (|x|<1) \\ (D^2-k^2)\, u_p^{n+1} &= \zeta_p^{n+1} \qquad (|x|<1) \\ u_p^{n+1} &= \zeta_p^{n+1} = 0 \qquad \text{at } x = \pm 1 \end{aligned} \tag{3.12}$$

and the Green's functions $u_\pm$ are determined in a preprocessing step as solutions to

$$\begin{aligned} &\frac{1}{\Delta t}\zeta_\pm - \nu(D^2-k^2)\zeta_\pm = 0 \qquad (|x|<1) \\ &(D^2-k^2)u_\pm = \zeta_\pm \qquad (|x|<1) \\ &u_\pm = 0, \quad \zeta_- = 0, \quad \zeta_+ = 1 \quad \text{at } x=+1 \\ &u_\pm = 0, \quad \zeta_- = 1, \quad \zeta_+ = 0 \quad \text{at } x=-1 \end{aligned} \tag{3.13}$$

Here $\alpha_\pm^{n+1}$ are determined by the constraints

$$Du_p^{n+1} + \alpha_+^{n+1} Du_+ + \alpha_-^{n+1} Du_- = 0 \qquad \text{at } x = \pm 1 \tag{3.14}$$

If $u_\pm$ are stored, the solution of (3.4) by this algorithm requires only the computational work of solving the two Helmholtz (or Poisson) equations (3.12) and (3.13). If storage is not available for the complete $u_\pm$ fields, only the boundary values $Du_\pm$ $(x=\pm 1)$ need be stored. In this case, one first solves (3.12) for u_p^{n+1}, then (3.14) for $\alpha_\pm^{n+1}$, and finally (3.12) once more for u^{n+1} with the modified boundary conditions

$$u^{n+1} = 0, \qquad \zeta^{n+1} = \alpha_\pm^{n+1} \qquad \text{at } x = \pm 1 \tag{3.15}$$

This involves about the same work as solving four Poisson equations.

4. FRACTIONAL TIME STEP (SPLITTING) METHODS

The implicit schemes described in Section 3 are easy enough to implement in one-dimensional (or separable) problems. However, in more complex geometries, they lead to difficult coupled computational problems, equivalent to that of solving for steady Stokes flow at each time step. Therefore, it is important to seek other, more efficiently solvable methods. This can be done by decoupling the pressure computation from that of the velocity, thereby reducing the problem from the solution of a (vector) fourth (or sixth) order equation to a system of separately solvable second-order equations. One way to do this is by use of fractional-step methods.

4.1. Velocity–Pressure Splitting with Normal Velocity Boundary Conditions

Here the time-differencing scheme involves two split (or fractional) time steps (Gottlieb and Orszag, 1977; Orszag and Kells, 1980). The first step involves solution of the inviscid equations

$$\frac{u^* - u^n}{\Delta t} = -Dp^{n+1} \tag{4.1}$$

$$\frac{v^* - v^n}{\Delta t} = -ikp^{n+1} \tag{4.2}$$

$$Du^* + ikv^* = 0 \tag{4.3}$$

for $|x| < 1$ with boundary condition

$$u^* = 0 \qquad (x = \pm 1) \tag{4.4}$$

(Note that the asterisk here does *not* signify complex conjugation.) The second step involves the solution of the viscous equations

$$\frac{u^{n+1} - u^*}{\Delta t} = \nu(D^2 - k^2)\, u^{n+1} \tag{4.5}$$

$$\frac{v^{n+1} - v^*}{\Delta t} = \nu(D^2 - k^2)\, v^{n+1} \tag{4.6}$$

for $|x| < 1$ with boundary conditions

$$u^{n+1} = v^{n+1} = 0 \qquad (x = \pm 1) \tag{4.7}$$

In this scheme, u^n and v^n do not satisfy the incompressibility constraint (2.3), although the intermediate variables u^* and v^* do. In comparison with the implicit coupled schemes of Section 3, the present splitting method has the advantage that it involves only the solution of second-order Helmholtz (or Poisson) equations in arbitrary geometries. In general geometries, splitting offers significant simplifications compared to unsplit schemes. However, as will be shown below, the splitting schemes suffer from large time-stepping errors if $\nu\, \Delta t$ is large that can only be removed by the more sophisticated methods to be introduced later.

It is by no means obvious that the splitting scheme (4.1)–(4.7) has solutions consistent with (and convergent to) the solutions of the Stokes equations. To highlight the difficulty, consider the following argument. It follows from (4.1) and the boundary conditions that

$$Dp^{n+1} = 0 \qquad (x = \pm 1) \tag{4.8}$$

but (2.1) gives

$$Dp = \nu D^2 u \qquad (x = \pm 1) \tag{4.9}$$

which is, in general, not vanishing. It may seem that there is an $O(1)$ error in the split pressure p^n as $\Delta t \to 0$ at the boundaries $x = \pm 1$.

In fact, the following error estimates hold for the scheme (4.1)–(4.7). The global error estimates

$$u^n(x) - u(x, n\,\Delta t) \approx u_1(x)\,\Delta t + O(\Delta t^{3/2}) \tag{4.10}$$

$$v^n(x) - v(x, n\,\Delta t) \approx v_1(x)\,\Delta t + O(\Delta t^{3/2}) \tag{4.11}$$

$$p^n(x) - p(x, n\,\Delta t) \approx p_1(x)\,\Delta t + O(\Delta t^{3/2}) \tag{4.12}$$

hold for fixed x with $|x| < 1$ as $\Delta t \to 0$, where u_1, v_1, and p_1 are finite functions of x. Near the boundaries $x = \pm 1$, the error estimates (4.10) and (4.11) hold together with

$$Du^n(x) - Du(x, n\,\Delta t) = O(\Delta t^{1/2}) \tag{4.13}$$

$$D^2u^n(x) - D^2u(x, n\,\Delta t) = O(1) \tag{4.14}$$

$$D^2v^n(x) - D^2v(x, n\,\Delta t) = O(\Delta t^{1/2}) \tag{4.15}$$

$$p^n(x) - p(x, n\,\Delta t) = O(\Delta t^{1/2}) \tag{4.16}$$

for $|x| - 1 = O[(\nu\,\Delta t)^{1/2}]$, while the error in Dp^n is, as noted above, $O(1)$ in this region. We also remark that the intermediate (split) velocities u^* and v^* do *not* exhibit the boundary layer structure (4.13)–(4.15). The velocities u^* and v^* give uniform $O(\Delta t)$ approximations to $u(x, n\,\Delta t)$ and $v(x, n\,\Delta t)$, respectively. Also, $p^n - \nu\,\Delta t\,\nabla^2 p^n$ does not exhibit the boundary layer structure and is a uniform $O(\Delta t)$ approximation to the pressure. These results are established in Section 5.

The error estimates (4.13)–(4.16) can be understood heuristically as follows. On the inviscid fractional step (4.1)–(4.4), incompressibility is imposed, but a slip velocity of order Δt is generated at the wall. In the following viscous step, the slip velocity is reduced to zero, but a boundary layer of thickness $O[(\nu\,\Delta t)^{1/2}]$ remains, inducing the errors (4.13)–(4.16).

Higher order methods, such as Crank–Nicolson time differencing, do not lead to higher order results with this splitting, because errors are dominated by the splitting error due to the noncommutativity of the inviscid pressure and viscous fractional steps.

4.2. Velocity–Pressure Splitting with Tangential Velocity Boundary Conditions

The previous scheme may be modified by replacing the normal velocity boundary condition (4.4) in the inviscid pressure step by

$$v^* = 0 \qquad (x = \pm 1) \tag{4.17}$$

In this case, the errors in the modes and their growth rates are $O(\Delta t^{1/2})$ even in the interior of the domain, so the method gives quite poor results, although the method is stable.

4.3. Velocity–Pressure Splitting with Viscous Boundary Conditions

It may be thought that the boundary errors in the splitting methods in Sections 4.1 and 4.2 originate from the boundary condition (4.4), which leads to (4.8) instead of (4.9) at $x = \pm 1$. Suppose that the splitting method in Section 4.1 is used with (4.4) replaced by the seemingly more accurate boundary condition

$$Dp^{n+1} = \nu D^2 u^n \tag{4.18}$$

which follows by evaluating the normal component of the Navier–Stokes equation (2.1) at $x = \pm 1$. Unfortunately, this is not an improvement. The spatial structure of the error for this method is *identical* to that of the splitting method with $u^* = 0$. This follows because (4.1) and (4.5) with $u^n = u^{n+1} = 0$ give

$$Dp^{n+1} = -\frac{u^*}{\Delta t} = \nu D^2 u^{n+1}$$

at the boundaries, so $D^2 u^n = D^2 u^{n+1}$. For any normal mode (3.5) with $\kappa \neq 1$, this implies that $D^2 u^n \equiv 0$, so $Dp^{n+1} = 0$ at the boundaries. (Using the arguments of Section 5, it may be shown that the mode with $\kappa = 1$ has $u^n = p^n \equiv 0$.)

It may seem that the boundary condition

$$Dp^{n+1} = \nu D^2 u^{n+1} \tag{4.19}$$

would lead to more accurate results. However, this boundary condition leads to coupled equations for p^{n+1} and u^{n+1}. Also, at least for semidiscrete schemes, the resulting scheme is not numerically stable.

4.4. Explicit Pressure Computation

The pressure is frequently obtained by solving a Poisson equation derived from the incompressibility constraint. Thus, we consider the scheme

$$D^2 p^{n+1} - k^2 p^{n+1} = \frac{Du^n + ikv^n}{\Delta t} \qquad (|x| < 1) \tag{4.20}$$

$$Dp^{n+1} = \nu(D^2 u^n - k^2 u^n) \qquad (x = \pm 1) \tag{4.21}$$

$$\frac{u^{n+1}-u^n}{\Delta t} = -Dp^{n+1} + \nu(D^2u^{n+1} - k^2u^{n+1}) \qquad (|x|<1) \qquad (4.22)$$

$$\frac{v^{n+1}-v^n}{\Delta t} = -ikp^{n+1} + \nu(D^2v^{n+1} - k^2v^{n+1}) \qquad (|x|<1) \qquad (4.23)$$

$$u^{n+1} = v^{n+1} = 0 \qquad (x = \pm 1) \qquad (4.24)$$

This scheme is analogous to one proposed by Harlow and Welch (1965). Again, the properties of normal modes of (4.20)–(4.24) are *identical* to those of the splitting method in Section 4.1, because $Dp^{n+1} = \nu D^2u^n$ by (4.21), but $Dp^{n+1} = \nu D^2u^{n+1}$ by (4.22) at the boundaries.

5. NORMAL MODE ANALYSIS

The methods introduced in Section 4 may be analyzed for both stability and accuracy using a normal mode analysis. That is, we shall seek normal mode solutions to the semidiscrete equations that are analogous to the normal modes (2.5) with (2.7)–(2.11) of the continuous model problem of Section 2. The corresponding normal modes are of the form (3.5),

$$(u^n(x), v^n(x), p^n(x)) = \kappa^n(\hat{u}(x), \hat{v}(x), \hat{p}(x)) \qquad (5.1)$$

where κ is the amplification factor. The semidiscrete approximation is stable if

$$|\kappa| \leqslant 1 + O(\Delta t) \qquad (5.2)$$

for all normal modes and is unstable otherwise. The accuracy of the particular semidiscrete method may be studied by computing the exponential growth rate $\tilde{\sigma}$, defined by

$$\kappa^n = \exp(\tilde{\sigma} n\, \Delta t), \qquad \tilde{\sigma} = \frac{1}{\Delta t} \ln \kappa \qquad (5.3)$$

The error $\tilde{\sigma} - \sigma$, where σ is given by (2.9)–(2.11), measures the time discretization error.

To analyze the fractional step methods of Section 4, the results (4.10)–(4.16) are established first for the normal modes of the system. The general results (4.10)–(4.16) then follow from completeness of the normal modes. A solution to (4.1)–(4.7) is sought in the form

$$(u^n, v^n, p^n) = \kappa^n(\tilde{u}, \tilde{v}, \tilde{p}) \qquad (5.4)$$

$$(u^*, v^*) = \kappa^n(\tilde{u}^*, \tilde{v}^*) \qquad (5.5)$$

Substituting (5.4) and (5.5) into (4.1)–(4.4) gives

$$(D^2-k^2)\,\tilde{u}^* = -ikD\tilde{v}-k^2\tilde{u} \tag{5.6}$$

while (4.5) and (4.6) give

$$\kappa\left[\frac{1}{\Delta t}-\nu(D^2-k^2)\right]\tilde{u}=\frac{1}{\Delta t}\,\tilde{u}^* \tag{5.7}$$

$$\kappa\left[\frac{1}{\Delta t}-\nu(D^2-k^2)\right]\tilde{v}=\frac{i}{k\,\Delta t}\,D\tilde{u}^* \tag{5.8}$$

The general form of the solution $\tilde{u}$, $\tilde{u}^*$ to (5.6)–(5.8) that is *symmetric* about $x=0$ is

$$\tilde{u}^*(x)=A\cosh kx+B\cos\tilde{\mu}x \tag{5.9}$$

$$\tilde{u}(x)=\frac{1}{\kappa}A\cosh kx+B\cos\tilde{\mu}x+C\cosh\lambda x \tag{5.10}$$

It also follows that

$$\tilde{v}(x)=\frac{i}{\kappa}A\sinh kx-\frac{i}{k}\tilde{\mu}B\sin\tilde{\mu}x+\frac{ik}{\lambda}C\sinh\lambda x \tag{5.11}$$

$$\kappa\tilde{p}(x)=-\frac{\kappa-1}{k\kappa\,\Delta t}A\sinh kx+\frac{1}{\lambda\,\Delta t}C\sinh\lambda x \tag{5.12}$$

Here

$$\tilde{\mu}=\left(-k^2-\frac{\kappa-1}{\nu\kappa\,\Delta t}\right)^{1/2} \tag{5.13}$$

and

$$\lambda=\left(k^2+\frac{1}{\nu\,\Delta t}\right)^{1/2} \tag{5.14}$$

The boundary conditions (4.4) and (4.7) are satisfied if the following determinant vanishes:

$$\begin{pmatrix} \cosh k & \cos\tilde{\mu} & 0 \\ (1/\kappa)\cosh k & \cos\tilde{\mu} & \cosh\lambda \\ (1/\kappa)\sinh k & -(\tilde{\mu}/k)\sin\tilde{\mu} & (k/\lambda)\sinh\lambda \end{pmatrix}=0 \tag{5.15}$$

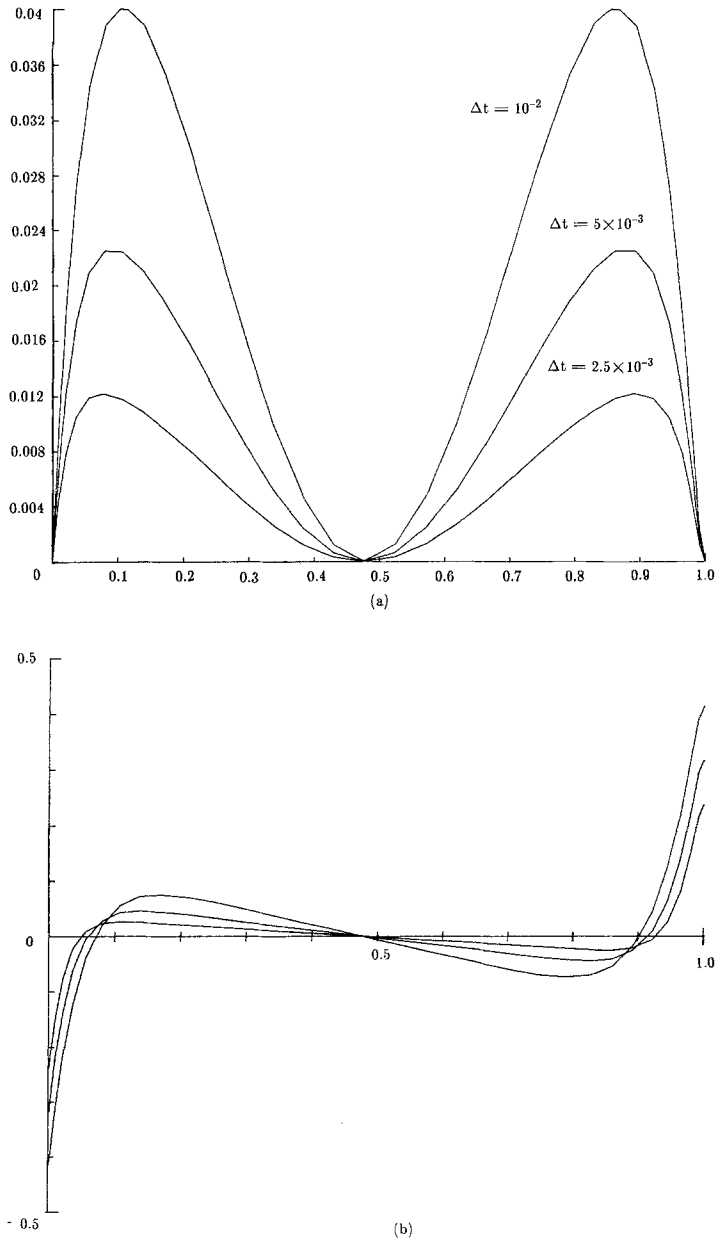

Fig. 2. Plots of the errors in the normal mode of the splitting scheme (4.1)–(4.7) with $\nu = k = 1$ with $\Delta t = 10^{-2}$, 5×10^{-3}, and 2.5×10^{-3}. (a) $\tilde{u}(x) - \hat{u}(x)$; (b) $\tilde{p}(x) - \hat{p}(x)$; (c) $D\tilde{p}(x) - D\hat{p}(x)$.

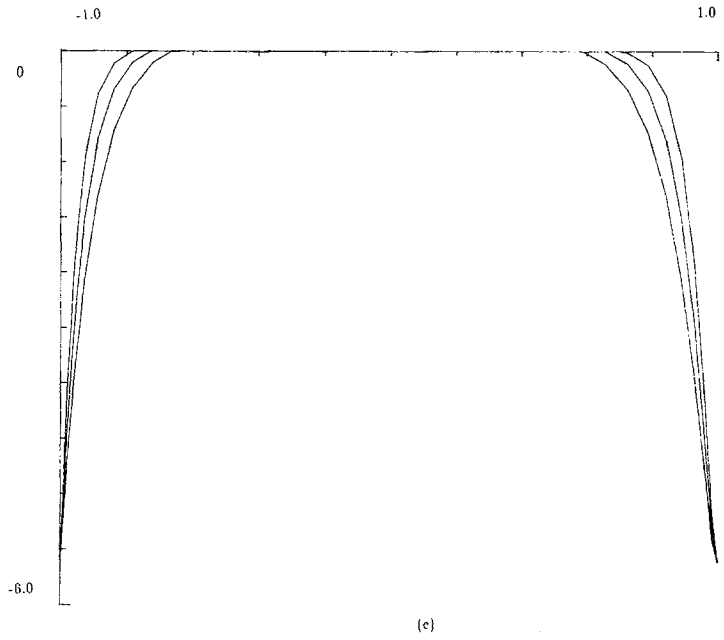

Fig. 2. Continued.

The limiting behavior of these normal modes as $\Delta t \to 0+$ is found as follows. First, the limiting form of (5.15) is, to within exponentially small correstions in Δt,

$$\frac{\tilde{\mu}}{k} \sin \tilde{\mu} \cosh k + \frac{1}{\kappa} \cos \tilde{\mu} \sinh k + \frac{k}{\lambda} \frac{\kappa - 1}{\kappa} \cos \tilde{\mu} \cosh k = 0 \qquad (5.16)$$

Writing

$$\kappa = 1 + \sigma \, \Delta t + O(\Delta t^2) \qquad (\Delta t \to 0+) \qquad (5.17)$$

and noting from (5.13) that $\tilde{\mu} \approx (-k^2 - \sigma/\nu)^{1/2}$, we obtain the leading-order dispersion relation

$$\left(-k^2 - \frac{\sigma}{\nu}\right)^{1/2} \tan \left(-k^2 - \frac{\sigma}{\nu}\right)^{1/2} + k \tanh k = 0 \qquad (5.18)$$

which is identical to (2.10). Thus, the leading behavior σ of the growth rate

$\tilde{\sigma}$ agrees with that of the exact solution. To higher order in Δt the solution to (5.15) is

$$\kappa = 1 + \sigma\,\Delta t + \Delta t^2\left(\frac{4\nu\sigma\mu\sin 2\mu}{\sin 2\mu + 2\mu} + \sigma^2\right) + \Delta t^{5/2}\left(\frac{4k^2\sigma\mu\nu^{3/2}\cos^2\mu}{\sin 2\mu + 2\mu}\right) + O(\Delta t^3) \tag{5.19}$$

where σ is a solution to (2.10) and μ is defined by (2.9).

From (5.9)–(5.12) and the result (5.19) for κ, it follows that, if we normalize the mode by assuming $A = \cos\mu$, then, as $\Delta t \to 0$,

$$B = -\cosh k = O(1) \tag{5.20}$$

$$C \approx 2\sigma\,\Delta t\cos\mu\cosh k\exp[-1/(\nu\,\Delta t)^{1/2}] \tag{5.21}$$

The estimates (4.10)–(4.16) follow immediately from (2.7), (5.20), (5.21), and the facts that

$$\cosh\lambda x\exp[-1/(\nu\,\Delta t)^{1/2}] = O(1)$$

when $|x| - 1 = O[(\nu\,\Delta t)^{1/2}]$ and is exponentially small otherwise and that $\tilde{\mu} - \mu = O(\Delta t) + O(\Delta t^{3/2})$. The boundary layer behavior is represented by the terms proportional to C in (5.11)–(5.13) for the normal modes. Since $C = O(\Delta t) \neq 0$, these normal modes exhibit a (weak) boundary layer behavior. Notice also that $\tilde{u}^*$ and $\tilde{v}^*$ have no boundary layer terms, showing that these intermediate results are uniform approximations to the normal modes of the exact dynamics.

In Table II, we list the decay rate $\tilde{\sigma}$ for the slowest decaying normal mode with $k = 1$ for this split step scheme. It is apparent that the error in $\tilde{\sigma}$

Table II. Decay Rate of Slowest Decaying Normal Mode of the Split-Step Scheme (4.1)–(4.7) with $k = 1$[a]

$\nu\,\Delta t$	$\tilde{\sigma}/\nu$
0.1	−7.3175
0.01	−9.0462
0.001	−9.2855
0.0001	−9.3109
0.+	−9.3137

[a] Here $\kappa = \exp(\tilde{\sigma}\,\Delta t)$.

behaves like Δt as $\Delta t \to 0+$. In Fig. 2, we plot the errors between the exact normal mode and that of the splitting method (3.11)–(3.17). It is apparent that the errors in Dp are significantly larger than in u, especially near the boundaries $x = \pm 1$.

6. EXTRAPOLATION METHODS

It is possible to reduce the error of the splitting methods introduced in Section 4 by applying local Richardson extrapolation methods. Let us consider first the solution to the initial-value problem

$$\partial u/\partial t = (A + B + C)\, u \tag{6.1}$$

where A, B, and C are (spatial) differential operators. A fully implicit splitting method (Yanenko, 1971) for solution of (6.1) is

$$\frac{u_1 - u(t)}{\Delta t} = Au_1 \tag{6.2}$$

$$\frac{u_2 - u_1}{\Delta t} = Bu_2 \tag{6.3}$$

$$\frac{u(t + \Delta t) - u_2}{\Delta t} = Cu(t + \Delta t) \tag{6.4}$$

The effect of the operators A, B, and C is accounted for separately in the three fractional steps (6.2)–(6.4). Under very general conditions, the scheme (6.2)–(6.4) is unconditionally stable and its solution converges to the solution of (6.1) as $\Delta t \to 0$ with global errors of order Δt. Higher order accuracy can be obtained by such variants of (6.2)–(6.4) as alternating-direction implicit methods. However, these latter methods are tricky when three or more operators $A, B, C,\ldots$ are involved, if the split operators do not commute, or if higher than second-order accuracy in time is desired.

A simple way to achieve high-order accuracy while maintaining unconditional stability is to extrapolate locally the error in (6.2)–(6.4). Denoting the solution to (6.2)–(6.4) as $u(t + \Delta t) \equiv L_{\Delta t} u(t)$, then a suitable Richardson extrapolant that leads to second-order global accuracy is

$$u(t + \Delta t) = (2L^2_{\Delta t/2} - L_{\Delta t})\, u(t) \tag{6.5}$$

This scheme requires roughly three times as much computational work as (6.2)–(6.4). Third-order accuracy is obtained using

$$u(t + \Delta t) = \frac{1}{3}\left[4(2L^2_{\Delta t/4} - L_{\Delta t/2})^2 - (2L^2_{\Delta t/2} - L_{\Delta t})\right] u(t) \tag{6.6}$$

which requires roughly seven times the work of the original scheme.

The unconditional stability of (6.5) is easily demonstrated for commutative operators A, B, and C by noting that, for the simple scalar equation $\partial u/\partial t = -\lambda u$, (6.5) gives

$$u(n\,\Delta t) = \left[2\left(\frac{1}{1+\frac{1}{2}\lambda\,\Delta t}\right)^2 - \frac{1}{1+\lambda\,\Delta t}\right]^n u(0) \tag{6.7}$$

so $|u(n\,\Delta t)| \leqslant |u(0)|$ for all $\Delta t > 0$ if $\operatorname{Re}\lambda \geqslant 0$.

The third-order method (6.6) is only conditionally stable for $\operatorname{Re}\lambda \geqslant 0$. There is a small region of instability when $\lambda\,\Delta t$ is nearly pure imaginary, with $0 \leqslant \operatorname{Im}\lambda\,\Delta t < 1.04$. The maximum growth rate of this instability is achieved for $\lambda\,\Delta t \approx 0 + 0.792i$; its growth rate is only κ^n with $\kappa \approx 1.00333$. This instability is so weak that it requires nearly 700 time steps to grow by a factor ten. An occasional stable explicit time step would stabilize the scheme and remove the effects of this instability. For larger values of $\lambda\,\Delta t$ and values away from the imaginary axis with $\operatorname{Re}\lambda < 0$, (6.6) is stable.

6.1. Extrapolated Implicit Time Stepping

If the time stepping scheme (4.1)–(4.7) is denoted symbolically as

$$u(t + \Delta t) = L_{\Delta t}\,u(t)$$

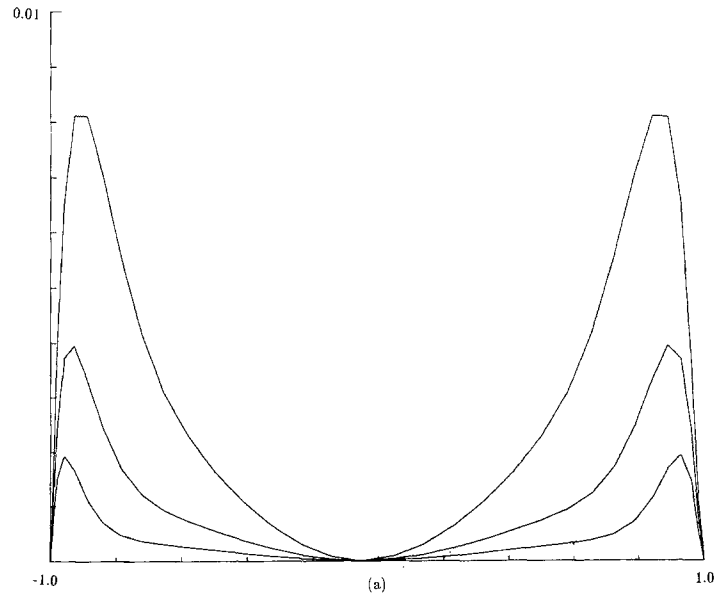

Fig. 3. Plots of the errors in the extrapolated splitting scheme (6.5) with $\Delta t = 0.01$, 5×10^{-3}, and 2.5×10^{-3}. (a) $u(x) - \hat{u}(x)$; (b) $p(x) - \hat{p}(x)$; (c) $Dp(x) - D\hat{p}(x)$.

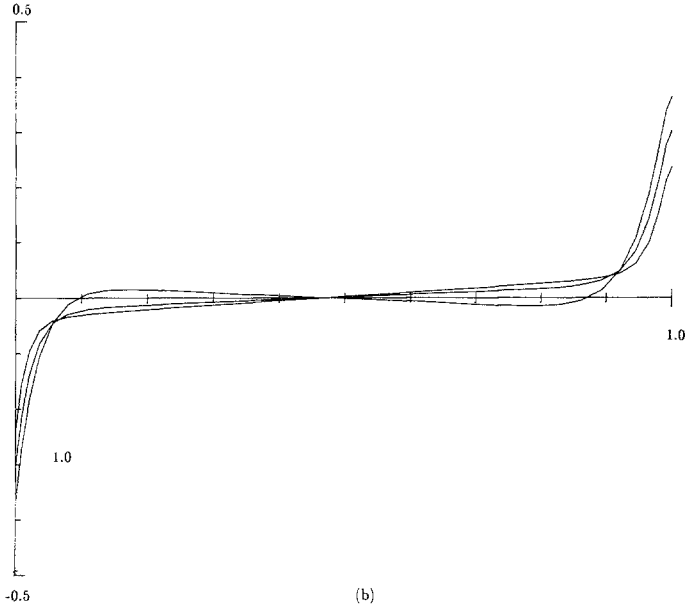

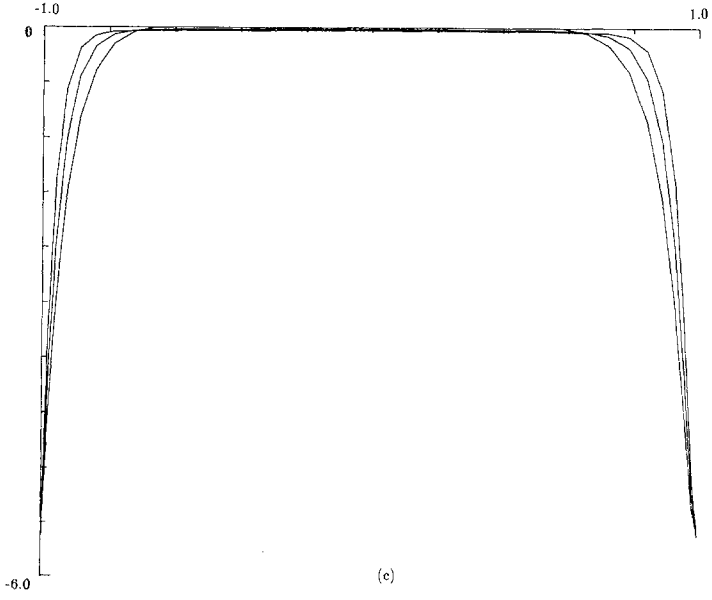

Fig. 3. Continued.

Table III. Decay Rate of Slowest Decaying Normal Mode of the Richardson Extrapolation (6.5) when $k = 1$

$\nu\,\Delta t$	$\tilde{\sigma}/\nu$
0.1	−9.06126
0.01	−9.30726
0.001	−9.31355
0.+	−9.31374

then the extrapolated scheme (6.5) removes the first-order (in Δt) errors of $u(t)$ while maintaining the unconditional stability of this implicit method. The error estimates (4.10)–(4.12) imply that the errors in this extrapolated scheme are of order $\Delta t^{3/2}$ for fixed x interior to the domain, but the boundary errors (4.13)–(4.16) remain unchanged. The normal-mode growth rate κ is now of the form

$$\kappa = e^{\sigma \Delta t} + O(\Delta t^{5/2}) \tag{6.8}$$

so the global time behavior is in error by $O(\Delta t^{3/2})$. In Table III, values of

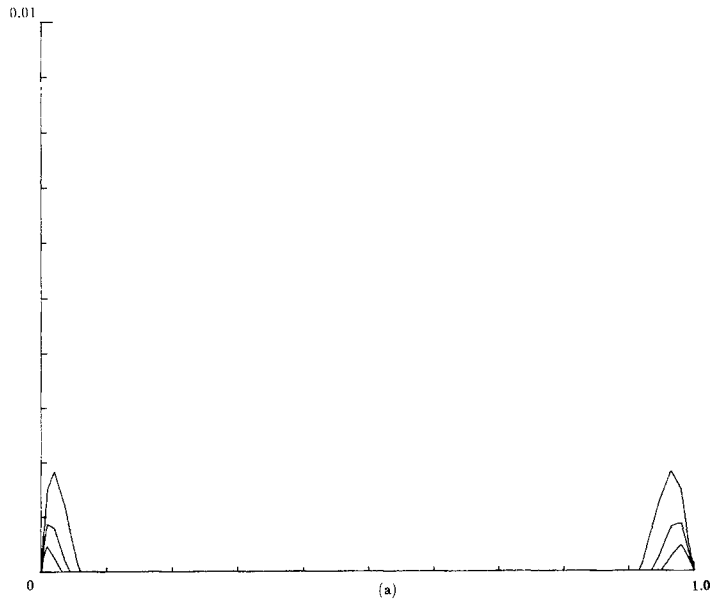

Fig. 4. Plots of the errors in the higher order extrapolated splitting scheme (6.9) with $\Delta t = 0.01$, 5×10^{-3}, and 2.5×10^{-3}. (a) $u(x) - \hat{u}(x)$; (b) $p(x) - \hat{p}(x)$; (c) $Dp(x) - D\hat{p}(x)$.

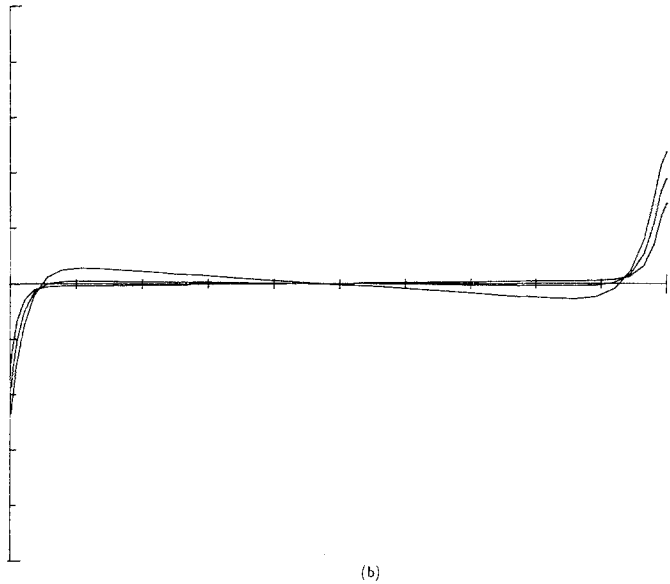

(b)

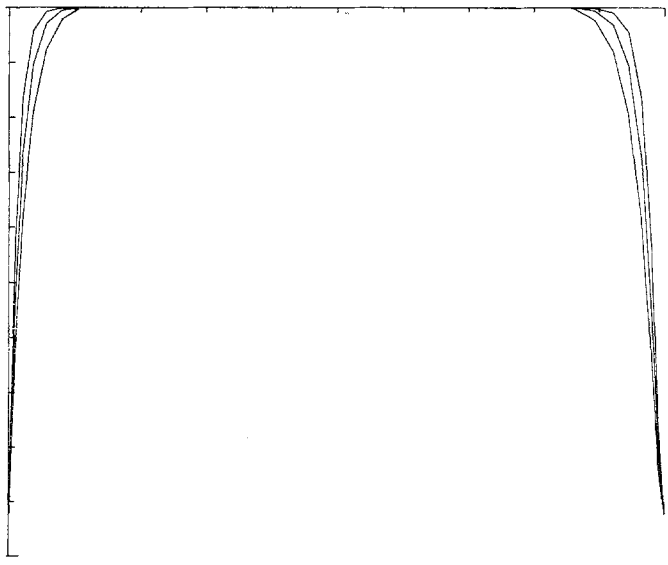

(c)

Fig. 4. Continued.

the decay rate $\tilde{\sigma}$ are listed for the slowest decaying mode when $k=1$. In Fig. 3, we plot the errors in the slowest decaying normal mode of this extrapolated splitting scheme.

6.2. Higher Order Extrapolated Implicit Time Stepping

Both the $O(\Delta t)$ and $O(\Delta t^{3/2})$ errors are eliminated by the higher order extrapolation scheme

$$u(t+\Delta t)=\frac{1}{2\sqrt{2}-1}\left[4\sqrt{2}\,(L_{\Delta t/4})^4-2(\sqrt{2}+1)(L_{\Delta t/2})^2+L_{\Delta t}\right]u(t) \tag{6.9}$$

The error in the scheme (6.9) is $O(\Delta t^2)$ for fixed x interior to the domain, while normal modes have growth rates of the form

$$\kappa=e^{\sigma\Delta t}+O(\Delta t^3) \tag{6.10}$$

The boundary error estimates (4.13)–(4.16) remain unchanged. Plots of the error in the slowest decaying normal mode for this scheme are given in Fig. 4. Decay rates for this mode are listed in Table IV.

Note that while these extrapolation schemes do remove interior errors as well as errors in the growth rates of normal modes, they do not remove either the boundary layer behavior of the splitting method or the $O(1)$ boundary errors in Dp.

7. REDUCED BOUNDARY DIVERGENCE METHODS

The problems with the splitting methods given in Section 4 originate with the appearance of nonsolenoidal (divergent) flow near the walls where the divergence condition $\nabla\cdot\mathbf{v}=0$ is dropped in favor of boundary con-

Table IV. Decay Rate of Slowest Decaying Normal Mode of the Second-Order Richardson Extrapolation (6.9) when $k=1$

$\nu\,\Delta t$	$\tilde{\sigma}/\nu$
0.1	−9.34337
0.01	−9.31391
0.001	−9.31374
0.+	−9.31374

ditions. In this section, we explore two classes of methods to alleviate this difficulty, namely, improved pressure boundary conditions and improved velocity boundary conditions.

7.1. Improved Pressure Boundary Conditions

7.1.1. Introduction

The boundary conditions (4.8), $Dp = 0$, on the splitting scheme of Section 4.1 are in error by $O(1)$, yet the resulting scheme is first-order in Δt in the interior of the domain [cf. (4.10)–(4.12)] and the pressure is determined to order $(\nu \Delta t)^{1/2}$ in the boundary region [cf. (4.16)]. In general, it appears that the pressure boundary condition can be one-half order less accurate in Δt than is required of the full scheme. Thus, while the first-order boundary condition (4.18), $Dp = \nu D^2 u^n$, does not lead to improved results with the first-order splitting scheme of Section 4.3, it does lead to second-order results with the second-order splitting

$$\frac{u^* - u^n}{\Delta t} = -Dp^{n+1/2} \tag{7.1}$$

$$\frac{v^* - v^n}{\Delta t} = -ikp^{n+1/2} \tag{7.2}$$

$$Du^* + ikv^* = 0 \tag{7.3}$$

$$\frac{u^{n+1} - u^*}{\Delta t} = \frac{1}{2}\nu(D^2 - k^2)(u^{n+1} + u^*) \tag{7.4}$$

$$\frac{v^{n+1} - v^*}{\Delta t} = \frac{1}{2}\nu(D^2 - k^2)(v^{n+1} + v^*) \tag{7.5}$$

Here we impose the boundary conditions

$$u^{n+1} = v^{n+1} = 0 \tag{7.6}$$

$$Dp^{n+1/2} = \nu D^2 u^n \tag{7.7}$$

Indeed, the normal modes of (7.1)–(7.5) have the form (5.9)–(5.11) with (5.13) and (5.14) replaced by

$$\lambda^2 = k^2 + \frac{2}{\nu \Delta t}, \qquad \tilde{\mu}^2 = -\frac{2}{\nu \Delta t}\frac{\kappa - 1}{\kappa + 1} - k^2 \tag{7.8}$$

Also, $p^{n+1/2} = \kappa^n \tilde{p}(x)$, with

$$\tilde{p}(x) = -\frac{\kappa - 1}{\kappa k\, \Delta t} A \sinh kx + \frac{1}{\lambda\, \Delta t} C \sinh \lambda x \tag{7.9}$$

analogous to (5.12). In this case, the matrix eigenvalue condition (5.15) becomes

$$\begin{bmatrix} -\left(\dfrac{\kappa - 1}{\kappa\, \Delta t} + \dfrac{\nu k^2}{\kappa}\right) \cosh k & \nu\tilde{\mu}^2 \cos \tilde{\mu} & \left(\dfrac{1}{\Delta t} - \nu\lambda^2\right) \cosh \lambda \\ \dfrac{1}{\kappa} \cosh k & \cos \tilde{\mu} & \cosh \lambda \\ \dfrac{1}{\kappa} \sinh k & -\dfrac{\tilde{\mu}}{k} \sin \tilde{\mu} & \dfrac{k}{\lambda} \sinh \lambda \end{bmatrix} = 0 \tag{7.10}$$

Therefore, to within exponentially small corrections in Δt, the dispersion relation is

$$\frac{\tilde{\mu}}{k} \cosh k \sin \tilde{\mu} + \frac{3 - \kappa}{\kappa + 1} \cos \tilde{\mu} \sinh k + 2 \frac{k}{\lambda} \frac{\kappa - 1}{\kappa + 1} \cos \tilde{\mu} \cosh k = 0 \tag{7.11}$$

The eigenvalue κ satisfies

$$\kappa = 1 + \sigma\, \Delta t + \frac{1}{2} \sigma\, \Delta t^2 + O(\Delta t^{5/2}) \tag{7.12}$$

so the effective growth rate is *accurate* to $O(\Delta t)$. For this method there is a numerical boundary layer, but the interior solution has errors of order Δt^2.

7.1.2. Improved Pressure Boundary Conditions

An arbitrary velocity field can be decomposed into its irrotational and solenoidal components $\mathbf{v}_I$ and $\mathbf{v}_S$, respectively:

$$\mathbf{v} = \mathbf{v}_I + \mathbf{v}_S \tag{7.13}$$

where

$$\begin{aligned} \nabla \times \mathbf{v}_I &= 0 \\ \nabla \cdot \mathbf{v}_S &= 0 \end{aligned} \tag{7.14}$$

Therefore, the boundary condition $\partial p/\partial n = \nu \mathbf{n} \cdot \nabla^2 \mathbf{v}$ can be rewritten

$$\frac{\partial p}{\partial n} = \nu \mathbf{n} \cdot [\nabla(\nabla \cdot \mathbf{v}) - \nabla \times (\nabla \times \mathbf{v})] = \nu \mathbf{n} \cdot \nabla(\nabla \cdot \mathbf{v}_I) - \nu \mathbf{n} \cdot [\nabla \times (\nabla \times \mathbf{v}_S)] \tag{7.15}$$

Since $\mathbf{v}_\tau$ may be assumed to vanish in incompressible flow, it is logical to replace the boundary condition (1.5) by the equivalent condition

$$\partial p/\partial n = -\nu \mathbf{n} \cdot [\nabla \times (\nabla \times \mathbf{v})] \tag{7.16}$$

For the model problem of Section 2, this modification of (1.5) becomes

$$Dp = -\nu(v_{xy} - u_{yy}) = -ivk(Dv - iku) \tag{7.17}$$

When the boundary condition

$$Dp^{n+1/2} = -ivkDv^n \tag{7.18}$$

(since $u^n = 0$) is used in place of (7.7), the matrix (7.10) is replaced by

$$\begin{bmatrix} -\left(\dfrac{\kappa - 1}{\kappa\, \Delta t} + \dfrac{\nu k^2}{\kappa}\right) \cosh k & \nu\tilde{\mu}^2 \cos\tilde{\mu} & \left(\dfrac{1}{\Delta t} - \nu k^2\right) \cosh\lambda \\ \dfrac{1}{\kappa} \cosh k & \cos\tilde{\mu} & \cosh\lambda \\ \dfrac{1}{\kappa} \sinh k & -\dfrac{\tilde{\mu}}{k} \sin\tilde{\mu} & \dfrac{k}{\lambda} \sinh\lambda \end{bmatrix} = 0 \tag{7.19}$$

To within exponentially small factors in Δt, the dispersion relation (7.19) is

$$\kappa \frac{\tilde{\mu}}{k} \sin\tilde{\mu} \cosh k + \frac{3\kappa - 1}{\kappa + 1} \cos\tilde{\mu} \sinh k + \frac{k}{\lambda} \frac{(\kappa - 1)^2}{\kappa + 1} \cos\tilde{\mu} \cosh k = 0 \tag{7.20}$$

Now it is easy to see that, in contrast to (7.12),

$$\kappa = 1 + \sigma\, \Delta t + \frac{1}{2} \sigma^2\, \Delta t^2 + O(\Delta t^3) \tag{7.21}$$

so the error in the growth rate is $O(\Delta t^2)$, in contrast to the error $O(\Delta t^{3/2})$ in (7.12). The use of the tangential derivative boundary condition (7.16) gains a factor $(\Delta t)^{1/2}$ in accuracy over the normal derivative boundary condition (7.7). In Table V, values of the decay rate $\tilde{\sigma}$ are listed for the slowest decaying modes with $k = 1$.

7.2. Higher Order Pressure Boundary Conditions

With the high-order time-difference scheme (1.11), it suffices to supply boundary conditions for the Poisson equation (1.13) or (1.15). With tangential boundary derivative conditions of the form (7.16), the order of accuracy of the boundary derivative can be chosen one order less than the

Table V. Decay Rates of the Slowest Decaying Normal Mode of the Pressure (7.1)–(7.6), (7.18) with $k = 1$

$\nu\,\Delta t$	$\tilde{\sigma}/\nu$
0.1	−13.31925
0.05	−9.72680
0.025	−9.40409
0.01	−9.32743
0.005	−9.31712
0.0025	−9.31458
0.001	−9.31385
0.+	−9.31374

desired interior error. However, this must be done consistently so that stability of the discrete approximation is maintained. Thus, to obtain third-order interior accuracy, we could choose

$$\frac{\partial p^{n+1}}{\partial n} = \frac{\partial p^n}{\partial n} + \Delta t \frac{\partial^2 p^n}{\partial t\,\partial n} + O(\Delta t^2)$$

$$= \frac{\partial p^n}{\partial n} - \nu\,\Delta t\,\nabla \times \left(\nabla \times \frac{\mathbf{v}^n - \mathbf{v}^{n-1}}{\Delta t} \right) + O(\Delta t^2) \tag{7.22}$$

For this scheme, the boundary layer structure of $Q = \nabla \cdot v$ implies that

$$Q|_{\partial D} = O(\sqrt{\nu}\,\Delta t^{5/2})$$

However, with this scheme there will be a slow numerical instability; indeed, with (7.22), there are nonzero normal modes satisfying $\kappa = 1$. This weak instability is easily eliminated by the iteration schemes outlined below; for example, we may modify (7.22) as in

$$\frac{\partial p^{n+1}}{\partial n} = \frac{\partial p^n}{\partial n} - \nu\,\Delta t\,\nabla \times \left(\nabla \times \frac{\mathbf{v}^n - \mathbf{v}^{n-1}}{\Delta t} \right) - \alpha \frac{\partial}{\partial n} \nabla \cdot \mathbf{v}^n \tag{7.23}$$

to remove the instability.

More generally, the boundary conditions for $\partial p/\partial n$ allow significant control of the boundary values of $Q^{n+1} = \nabla \cdot \mathbf{v}^{n+1}$. For the continuum problem, (7.16) holds. However, for a divergent velocity field, (7.16) reverts to (7.15) in the form

$$\left.\frac{\partial p}{\partial n}\right|_{\partial D} = \nu \left.\frac{\partial Q}{\partial n}\right|_{\partial D} - \nu \mathbf{n} \cdot \nabla \times (\nabla \times \mathbf{v})|_{\partial D} \tag{7.24}$$

The boundary condition (7.24) suggests an iteration scheme to remove the boundary errors. Suppose we solve (1.13) with the boundary conditions

$$\left.\frac{\partial p^{n+1,k+1}}{\partial n}\right|_{\partial D} = \left.\frac{\partial p^{n+1,k}}{\partial n}\right|_{\partial D} - \alpha \left.\frac{\partial Q^{n+1,k}}{\partial n}\right|_{\partial D} \tag{7.25}$$

where k is the iteration index at level $n+1$ and α is an iteration parameter. It may be shown that, for suitable choice of α, this iteration converges so that $\partial Q^{n+1,\infty}/\partial n = 0$. Therefore, the iteration method (7.25) maintains incompressibility, including the walls, so that the Navier–Stokes equations are satisfied throughout the computational domain.

Solution of the Poisson equation (1.13) for p^{n+1} with the Neumann boundary conditions (7.25) requires that a compatibility condition hold. It is required that

$$\oiint_{\partial D} \frac{\partial p^{n+1,k+1}}{\partial n}\, d\sigma = \oiint_{\partial D} \left[\frac{\partial p^{n+1,k}}{\partial n} - \alpha \frac{\partial Q^{n+1,k}}{\partial n}\right] d\sigma$$

$$= \iiint_D \left(\frac{Q^n}{\Delta t} + \nabla \cdot \mathbf{F}^n\right) dV$$

For this to hold for all k, it is necessary that

$$\oiint_{\partial D} \frac{\partial Q^{n+1,k}}{\partial n}\, d\sigma = 0$$

which holds because (1.12) implies that

$$\oiint_{\partial D} \frac{\partial Q^{n+1,k}}{\partial n}\, d\sigma = \iiint_D \nabla^2 Q^{n+1,k}\, dV$$

$$= \iiint_D \frac{Q^{n+1,k}}{\nu\, \Delta t}\, dV = \oiint_{\partial D} \frac{\mathbf{v}^{n+1,k} \cdot \mathbf{n}}{\nu\, \Delta t}\, d\sigma = 0$$

7.3. Improved Velocity Boundary Conditions

Kim and Moin (1985) observed that replacement of the viscous boundary conditions (4.7) in the split scheme (4.1)–(4.6) by

$$u^{n+1} = \Delta t\, Dp^{n+1} \qquad (x = \pm 1) \tag{7.26}$$

$$v^{n+1} = ik\, \Delta t\, p^{n+1} \qquad (x = \pm 1) \tag{7.27}$$

improves the accuracy of the scheme. Unfortunately, the boundary con-

ditions (7.26)–(7.27) allow a mode with $\kappa = 1$, so the scheme is weakly unstable. However, (4.1) and (4.4) imply that

$$u^{n+1}/\Delta t = Dp^{n+1} = u^n/\Delta t$$

so $u^n = 0$ if $\kappa \neq 1$. The improved boundary conditions

$$u^{n+1} = 0, \qquad v^{n+1} = ik\,\Delta t\, p^{n+1} \tag{7.28}$$

remove the instability and give more accurate results. This formulation of the velocity boundary conditions was given by Zang and Hussaini (1986) and Fortin *et al.* (1971).

Let us illustrate this scheme for the Crank–Nicolson method (7.1)–(7.5) with the boundary conditions

$$u^* = u^{n+1} = 0, \qquad v^{n+1} = ik\,\Delta t\, p^{n+1/2} \tag{7.29}$$

The matrix eigenvalue condition is then

$$\begin{bmatrix} \cosh k & \cos\tilde{\mu} & 0 \\ \dfrac{1}{\kappa}\cosh k & \cos\tilde{\mu} & \cosh\lambda \\ \dfrac{2\kappa-1}{\kappa}\sinh k & -\dfrac{\tilde{\mu}\kappa}{k}\sin\tilde{\mu} & \dfrac{(\kappa-1)\,k}{\lambda}\sinh\lambda \end{bmatrix} = 0 \tag{7.30}$$

To within exponentially small factors in Δt, the dispersion relation is

$$\frac{\tilde{\mu}}{k}\kappa \sin\tilde{\mu}\cosh k + \frac{2\kappa-1}{\kappa}\cos\tilde{\mu}\sinh k + \frac{(\kappa-1)^2\,k}{\kappa\lambda}\cos\tilde{\mu}\cosh k = 0 \tag{7.31}$$

Table VI. Decay Rate of the Slowest Decaying Normal Mode of the Improved Velocity Boundary Condition Scheme (7.1)–(7.5), (7.29)

$\nu\,\Delta t$	$\tilde{\sigma}/\nu$
0.05	−10.19966
0.025	−9.46642
0.01	−9.33509
0.005	−9.31889
0.0025	−9.31502
0.001	−9.31397
0.+	−9.31374

For small Δt, the expansion (7.21) holds once again. In Table VI, we list values of the decay rate $\tilde{\sigma}$ for the slowest decaying modes of this scheme with $k = 1$.

The present scheme is interesting in that it leads to second-order results for flow quantities at intermediate time steps, despite the fact that the full time-step boundary condition (7.28) is in error by $O(\Delta t)$.

8. CONCLUSIONS

In this paper, we have analyzed the effect of boundary conditions on incompressible flows. We have explained and analyzed a numerical boundary layer of thickness $(\nu \Delta t)^{1/2}$ that appears in many formulations of incompressible flow problems and we have explained techniques for the development of high-order methods.

For first- or second-order methods, we recommend the use of splitting methods in the form (4.1)–(4.5) or (7.1)–(7.5) with the tangential-derivative boundary conditions (7.16) or the modified velocity boundary conditions (7.28). To achieve higher order accuracy, we may employ either the extrapolation methods outlined in Section 6 or, perhaps even better, use schemes of the form (1.11) with high-order pressure boundary conditions of the form (7.23) or iterative conditions of the form (7.25) (with only a few iterations per time step).

We have shown that we can characterize methods for the solution of incompressible flow problems as belonging to either parabolic or elliptic type with regard to the determination of the pressure field. The elliptic schemes typically have smaller errors in the divergence field, with the errors decaying exponentially away from the boundaries of the computational domain. On the other hand, the parabolic schemes have smooth solutions, without numerical boundary layers, but care should be exercised with respect to the boundary conditions in order that initial divergence errors be eliminated. This analysis explains why "elliptic" schemes, such as that introduced by Harlow and Welch (1965), have been found to be more accurate than parabolic schemes.

We have also shown, using Weyl's lemma for the decomposition of a flow into its solenoidal and irrotational components, that it is possible to derive accurate boundary conditions for the pressure that involve only the tangential derivative of the boundary vorticity. This form of the boundary condition tends to minimize the effects of numerical boundary layers induced by splitting methods.

APPENDIX A. BOUNDARY-DIVERGENCE-FREE IMPLICIT TIME SPLITTING

Marcus (1984) uses a modification of the splitting scheme of Section 4.1 to remove the boundary errors discussed above. The idea is that splitting error induces large boundary errors because a large divergence of (u, v) develops near the boundaries $|x| = 1$ on the viscous step (see Section 5). This modified method is based on the observation that the normal flow boundary condition $u = 0$ is applied twice each time step in the splitting scheme of Section 4.1 [cf. (4.4) and (4.7)]. By modifying these conditions on u, it may be possible to reduce the error in the boundary divergence. The modified scheme is given by dropping the intermediate boundary condition (4.4), $u^* = 0$, in favor of the condition

$$Du^{n+1} + ikv^{n+1} = 0 \quad (x = \pm 1) \qquad \text{or} \qquad Du^{n+1} = 0 \quad (x = \pm 1) \tag{A1}$$

while applying (4.1)–(4.3) and (4.5)–(4.7). Thus, normal flow is allowed at the boundary during the inviscid pressure step in order to ensure that (A1) holds in the viscous step.

It may be shown by normal mode analysis (see Section 5) that this modified scheme gives results that are *identical* to those of the full implicit coupled scheme of Section 3.1, so there is *no* boundary layer behavior. The scheme is stable in time. Higher order differencing methods (such as Crank–Nicolson differencing) will yield higher order results for this method. However, the price paid for the removal of the boundary errors is that the boundary condition (A1) couples the pressure and viscous fractional steps, which makes the computational work similar to that of the full implicit coupled schemes. Indeed, this method may be implemented using the same Green's function ideas outlined in (3.11)–(3.15). For problems that are not separable, this work becomes unreasonably large. However, divergence-free boundary conditions may be imposed in an iteration scheme to minimize the computational work. We do not believe that this scheme is competitive with those of Section 7.

APPENDIX B. PENALTY METHOD

Here the method to solve (2.1)–(2.4) is, with the simplest implicit time-stepping,

$$\frac{u^{n+1} - u^n}{\Delta t} = -Dp^{n+1} + \nu(D^2 u^{n+1} - k^2 u^{n+1}) \tag{B1}$$

$$\frac{v^{n+1}-v^n}{\Delta t} = -ikp^{n+1} + \nu(D^2v^{n+1} - k^2v^{n+1}) \tag{B2}$$

$$\varepsilon p^{n+1} = -(Du^{n+1} + ikv^{n+1}) \tag{B3}$$

$$u^{n+1} = v^{n+1} = 0 \qquad (x = \pm 1) \tag{B4}$$

with $\varepsilon > 0$ chosen to minimize errors. This penalty method is a variant of the penalty method now widely used in finite-element methods (Temam, 1979). It is also closely related to the artificial compressibility method (Chorin, 1968; Temam, 1979). The dispersion relation for this scheme is

$$\tilde{\mu} \tan \tilde{\mu} + (k^2/\lambda) \tanh \tilde{\lambda} = 0 \tag{B5}$$

where $\tilde{\mu}$ is given by (5.13) and

$$\tilde{\lambda} = \left[k^2 + \frac{\varepsilon(\kappa - 1)}{\kappa \Delta t(1 + \nu\varepsilon)} \right]^{1/2} \tag{B6}$$

Thus, the modes of this scheme agree with the exact eigenmodes with errors of order ε, with no significant boundary errors. To minimize errors, ε should be chosen as small as possible, consistent with the stability of the fully discretized scheme in both space and time.

A quantitive measure of the accuracy of this method is obtained by writing

$$\kappa = (1 + \tilde{\rho}\nu \Delta t)^{-1} \tag{B7}$$

so the decay rate is

$$\frac{\tilde{\sigma}}{\nu} = -\frac{1}{\nu \Delta t} \ln(1 + \tilde{\rho}\nu \Delta t) \tag{B8}$$

In the limit $\nu \Delta t$, $\tilde{\sigma}/\nu \approx -\tilde{\rho}$, so the error in $\tilde{\rho}$ is a measure of the errors induced by the penalty parameter ε for small time steps. Some results are given in Table VII for $k = 1$ and 10.

In practice, the penalty method is not convenient for multidimensional problems, because it involves the solution of nonseparable equations for flow quantities at time step $n+1$. Also, for small ε, the equations at step $n+1$ are very stiff. For the Navier–Stokes equations, (B3) is replaced by the artificial compressibility relation

$$\varepsilon p + \nabla \cdot \mathbf{v} = 0 \tag{B9}$$

Table VII. Decay Rates of Slowest Decaying Normal Mode with $k = 1$ and 10, Using the Penalty Method (B1)–(B4)[a]–(A2.4)

	$\tilde{\rho}$	
$\nu\varepsilon$	$k = 1$	$k = 10$
0.1	8.947154	103.0083
0.01	9.280810	103.0361
0.001	9.313415	103.0394
0.000001	9.313737	103.0394
0.+	9.313742	103.0395

[a] Here $\tilde{\rho}$ is defined by (B7). Equation (B8) shows that $\tilde{\sigma}/\nu \approx -\tilde{\rho}$ as $\nu\,\Delta t \to 0+$.

where $\varepsilon > 0$ is the penalty parameter. If (B9) is substituted into the Navier–Stokes equation, one obtains

$$\frac{\partial \mathbf{v}}{\partial t} + \mathbf{v} \cdot \nabla \mathbf{v} = \frac{1}{\varepsilon} \nabla(\nabla \cdot \mathbf{v}) + \nu \nabla^2 \mathbf{v} \tag{B10}$$

Since the penalty parameter makes this problem very stiff for small ε, the time stepping scheme for (B10) should be strongly A-stable. Thus, full implicit rather than Crank–Nicolson schemas should be used to solve (B10).

ACKNOWLEDGMENTS

This work was supported by the Air Force Office of Scientific Research under grant 83-0089, the Office of Naval Research under contracts N00014-82-C-0451 and N00014-85-K-0201, and the National Science Foundation under grants ATM-8414410 and MSM-8514128.

REFERENCES

Chorin, A. J. (1968). *Math. Comp.* **23**, 341–354.

Fortin, M., Peyret, R., and Temam, R. (1971). *J. Mecanique* **10**, 357–390.

Gottlieb, D., and Orszag, S. A. (1977). In *Numerical Analysis of Spectral Methods*, SIAM, Philadelphia.

Gottlieb, D., Hussaini, M. Y., and Orszag, S. A. (1984). In Voigt, R. G., Gottlieb, D., and Hussaini, M. Y. (eds.), *Spectral Methods for Partial Differential Equations*, SIAM, Philadelphia, pp. 1–54.

Harlow, F. H., and Welch, J. E. (1965). *Phys. Fluids* **8**, 2182–2189.

Kim, J., and Moin, P. (1985). *J. Comp. Phys.* **59**, 308–323.
Kleiser, L., and Schumann, U. (1980). In Hirschell, E. H., *Proceedings Third GAMM Conference on Numerical Methods in Fluid Dynamics*, Vieweg, Braunschweig, pp. 165–173.
Marcus, P. S. (1984). *J. Fluid Mech.* **146**, 45–64.
Moin, P., and Kim, J. (1980). *J. Comp. Phys.* **35**, 381.
Orszag, S. A., and Israeli, M. (1974). *Annu. Rev. Fluid Mech.* **5**, 281–318.
Orszag, S. A., and Kells, L. (1980). *J. Fluid Mech.* **96**, 159–205.
Temam, R. (1979). *Navier–Stokes Equations*, North-Holland, Amsterdam.
Yanenko, N. N. (1971). *The Method of Fractional Steps*, Springer, New York.
Zang, T., and Hussaini, M. Y. (1986). *Appl. Math. Comp.*, to appear.

Printed in Belgium